els (GCMs) are currently being developed in several major research centers for simulating and predicting seasonal and interannual variability (e.g., Miyakoda et al. 1990; Philander et al. 1992; Latif et al. 1993; Ji and Leetmaa 1994; Robertson et al. 1995a; Robertson et al. 1995b). At the moment they have experienced some degree of difficulties (Neelin et al. 1992; Mechoso et al. 1995). Statistics of 11 coupled GCMs reveal a common problem in simulating the climatic asymmetry of relevance to the intertropical convergence zones (ITCZ; Mechoso et al. 1995).

Philander et al. (1992) successfully simulated ENSO-like interannual variability in their coupled model, which does not contain a seasonal cycle. Other models may simulate the seasonal cycle, but have little interannual variability. In general, the amplitudes of both seasonal and interannual variations are underestimated in many coupled models, although some progress has been made recently (e.g., Schneider et al. 1997; Frey et al. 1997; Ineson and Davey 1997).

Given that the seasonal cycle and the interannual oscillation interact nonlinearly with each other and that the annual-mean climate is critical in determining the seasonal cycle (Li and Philander 1996), it is conceivable that the annual mean state may play an important role on both seasonal and interannual variability in the Tropics. The goal of this study is to investigate the role of the annual-mean climate on seasonal and interannual variability by means of a coupled ocean–atmosphere GCM. This paper is organized as follows. In section 2 a coupled ocean–atmosphere model is briefly introduced. In section 3 we describe three sets of coupled experiments. In sections 4 and 5 we discuss, respectively, the role of the annual-mean climate on seasonal and interannual variations. A summary and further discussions are given in section 6.

2. Model

A coupled ocean–atmosphere general circulation model has been developed at the Naval Research Laboratory. This model has as its atmospheric component the Naval Operational Global Atmospheric Prediction System (NOGAPS; Hogan and Rosmond 1991) and as its oceanic component the Geophysical Fluid Dynamics Laboratory (GFDL) Modular Ocean Model (MOM; Pacanowski 1995).

The GFDL MOM has been widely used by many research groups for the study of climate dynamics and ocean–atmosphere interactions (e.g., Philander and Pacanowski 1981; Philander and Seigel 1985; Chao and Philander 1993; Manabe and Stouffer 1996). It is a three-dimensional primitive equation model, based on the original work by Bryan (1969). We currently use version MOM 2.0, which contains state-of-the-art physical parameterizations and numerical schemes, such as the implicit free surface (Dukowicz and Smith 1994), a conjugate gradient elliptic equation solver, the Richardson number dependent vertical mixing (Pacanowski and Philander 1981), and shortwave radiation penetration.

The ocean model has a uniform grid of 2° in longitude and a variable grid in latitude that has the finest resolution of 0.5° between 5°S and 5°N, gradually increases to 2° at 30°N and 30°S, and remains constant poleward. There are 25 vertical levels, with 10 levels equally distributed in the upper 100 m. The ocean model covers a region of 30°S–50°N and 0°–360°E. Along the northern and southern boundaries, temperature and salinity are restored (with a Newtonian damping timescale of 15 days) toward the seasonally varying Levitus (1982) climatology. Outside of the region the SST fields are specified from observations (Levitus 1982).

The atmospheric model (NOGAPS) uses a spectral transform method for horizontal calculations and an energy conserving finite difference method for the vertical. In the current study NOGAPS has a triangular resolution of T39, which corresponds to a horizontal resolution of 3° in both lat and long. The model has 12 vertical sigma levels. The advanced physics parameterizations include the solar and longwave radiation schemes (Harshvardhan et al. 1987), Slingo's (1987) cloud model, relaxed Arakawa and Schubert cumulus convection scheme (Moothi and Suarez 1992), shallow cumulus (Tiedtke 1984), Louis's surface flux parameterization and vertical mixing (Louis et al. 1982), large-scale condensation, gravity wave drag (Palmer et al. 1986), bucket model ground hydrology, and single soil level ground temperature prediction.

The atmosphere and ocean interact in such a way that the atmosphere influences the ocean through 1) shortwave solar radiation modified by clouds, 2) upward and downward longwave radiation at the ocean surface, 3) latent and sensible heat fluxes on the air–sea interface, 4) surface wind stress, and 5) fresh water fluxes, whereas the ocean affects the atmosphere through sea surface temperatures (that further change the surface moisture and heat distribution). A technique has been developed in such a way that different-resolution atmosphere and ocean models can be easily coupled through a simple interface, which automatically interpolates data from each model grid. The atmosphere and ocean can be coupled at any desired time intervals. In the current study we couple the atmosphere and ocean once per day. By doing so, we intentionally filter out the diurnal variation of SSTs.

3. Experiment designs

Three sets of coupled experiments have been designed in order to investigate the role of the annual mean climate on seasonal and interannual variability. In case A, no annual mean flux adjustment is applied. That is, the coupled model produces its own time-mean state without any flux correction. In case B, an annual-mean flux adjustment method is applied that ''corrects'' the annual

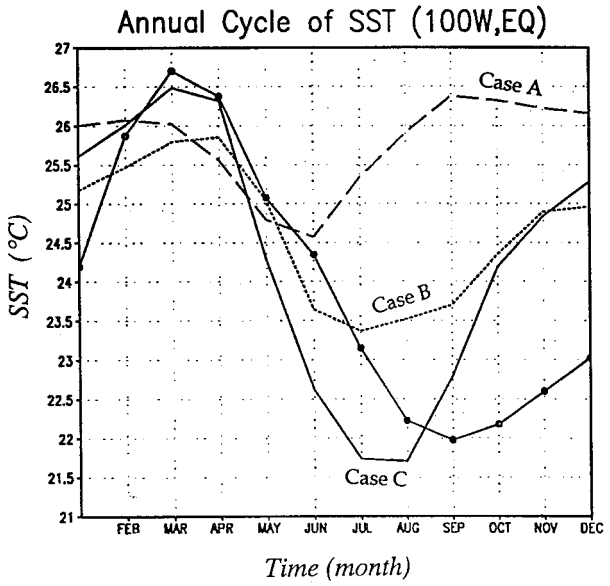

FIG. 1. Simulated annual cycles of SST (°C) at (0°N, 100°W) for case A (the dashed line), case B (the dotted line), and case C (the solid line). The solid circle line denotes the observed (COADS; Sadler et al. 1987) annual cycle at the same location.

mean SST field only. In case C, both the annual mean SST and surface wind fields are adjusted.

It is generally found that the coupled models gradually drift into a new climate equilibrium state that is far away from the observed climate. A possible way to prevent the model equilibrium state from departing too strongly from the observed equilibrium is to apply a flux adjustment method (Sausen et al. 1988). This flux adjustment can be either time dependent or independent. In their 1000-yr climate sensitivity experiments, Manabe and Stouffer (1996) adopted a seasonally varying flux adjustment method. By contrast, in this study we use a time-independent annual mean flux adjustment approach.

The procedures to compute the annual mean flux adjustment for SST are as follows: 1) We integrate the atmospheric model (NOGAPS) for 5 yr with prescribed observed seasonally varying SSTs. 2) We perform an average for the last 3 yr to obtain the annual mean atmospheric surface conditions (such as the annual mean surface wind stress and net surface heat flux fields). 3) In the ocean-only run, we force the ocean model (MOM) with the above annual mean atmospheric surface conditions. In this calculation a Newtonian damping term (with a restoring timescale of 10 days) is introduced in the SST equation that restores the model SST toward the observed annual-mean field. The annual-mean flux correction is finally diagnosed as the model reaches an equilibrium. 4) In the subsequent coupled runs, the diagnosed flux correction term is added into the SST equation, as an additional flux term. This flux correction term is only a function of space, and therefore does not damp seasonal and interannual variations. This method is different from the one used by Latif et al. (1988), who found that the climatic variability is considerably damped when a flux adjustment is applied.

The annual-mean surface wind is adjusted using the following approach. The error of the annual-mean surface wind field is first diagnosed from the uncoupled atmosphere-only run with the prescribed seasonally varying SSTs. Then in the coupled runs we simply add the difference between the observed and NOGAPS annual-mean surface wind into the model wind field, before it is used to force the ocean. Because of the wind difference, the annual-mean flux adjustment for SST needs to be recalculated for case C. The observed surface wind fields are obtained from the Comprehensive Ocean–Atmosphere Data Set (COADS; Sadler et al. 1987).

4. The seasonal cycle simulation

One of the principal mechanisms that control the seasonal cycle of SST is the response of the ocean to the seasonally varying solar radiation forcing. This mechanism can readily explain (to a large extent) the seasonal SST changes in most of world oceans, except in the Tropics where the air–sea interactions come into play.

Li and Philander (1996) show that the annual harmonic of solar radiation associated with the ellipticity of the earth's orbit is relatively unimportant for the annual cycle at the equator. The important forcing is the anitsymmetric solar radiation that is associated with the tilt of the earth's axis. Although it is zero at the equator, this antisymmetric solar radiation can force an annual SST variation at the equator through various air–sea feedback processes, provided the annual mean state of the coupled system contains an antisymmetric component.

The asymmetric annual-mean climate can permit an annual cycle at the equator, even in a model that couples the atmosphere to a one-dimensional mixed layer ocean (that means that there is no ocean dynamics involved). In such a model the northward winds at the equator will be stronger toward the end of the northern summer and relaxed toward the end of the northern winter (because the annual mean wind is southerly). Evaporation associated with these winds can cause the SST at the equator to be low in August and September, and high in March and April, and therefore forces an annual cycle at the equator. This air–sea feedback process can be simply represented by the first term on the right-hand side of a simplified SST equation,

$$\frac{\partial T'}{\partial t} \propto \alpha(|\overline{V} + V'| - |\overline{V}|) - w'\frac{\partial \overline{T}}{\partial z} - \left(v'\frac{\partial \overline{T}}{\partial y} + \overline{v}\frac{\partial T'}{\partial y}\right) - \beta C'_{\mathrm{STR}}, \qquad (4.1)$$

where T, V, w, v, and C_{STR} denote, respectively, SST,

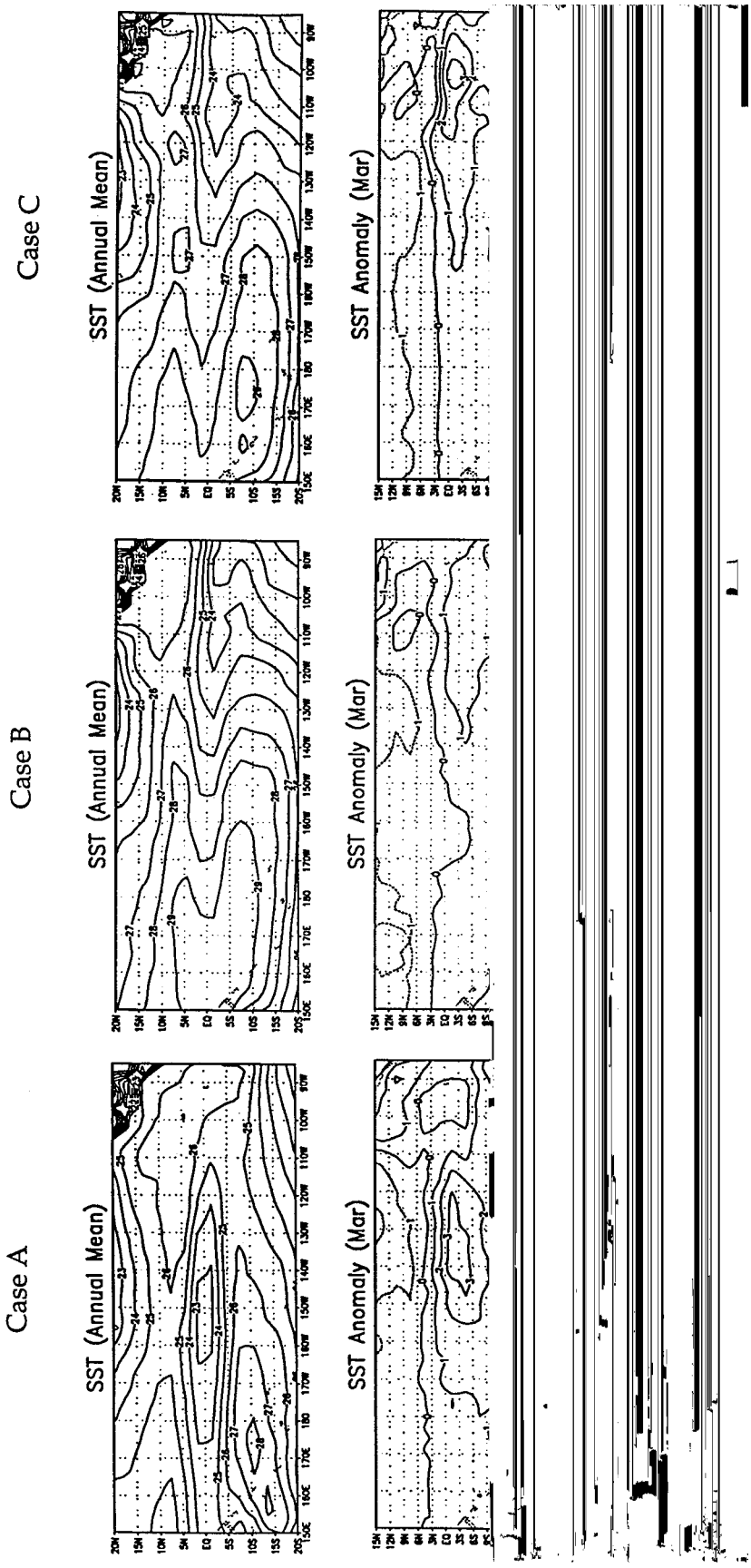

FIG. 2. Simulated annual-mean SSTs (the top panels) and SST variations (°C) in Mar (the middle panels) and Aug (the bottom panels) for cases A, B, and C.

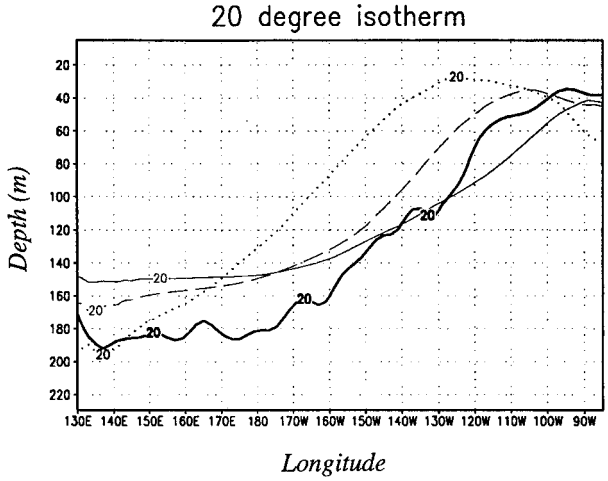

FIG. 3. Zonal structure of the ocean thermocline represented by 20°C isothermal along the equator in case A (the dotted line), case B (the dashed line), and case C (the thin solid line). The thick solid line represents the Levitus (1982) climatology.

the meridional wind at the surface, vertical velocity at the base of the ocean mixed layer, meridional surface ocean current, and low-level stratus cloud amount, and α and β are coefficients related to the surface evaporation and short-wave radiation. A variable with a bar denotes the annual-mean state and a prime denotes the departure from the mean. For the case of the evaporation–wind feedback only, if the annual mean state were perfectly symmetric about the equator (i.e., $\overline{V} = 0$), a semiannual rather annual variation in SST would occur.

The dynamic coupling between the ocean and atmosphere is another possible mechanism to change SST. The Chang–Philander (1994) coupled instability theory states that in response to a northward (southward) cross-equatorial wind, an equatorial antisymmetric cell is established that has anomalous upwelling to the south (north) of the equator and downwelling to the north (south). Since the strength of this coupled instability

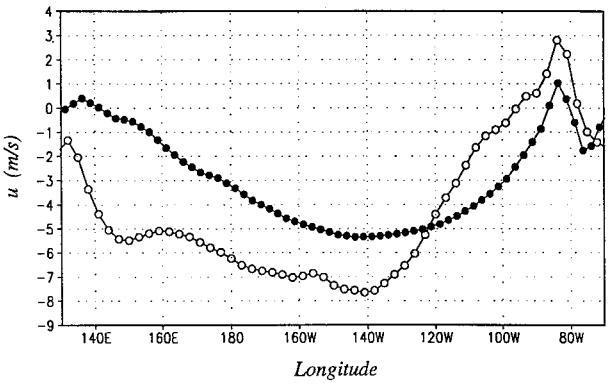

FIG. 4. Observed (close circles) and NOGAPS simulated (open circles, the uncoupled run) surface zonal wind component along the equator.

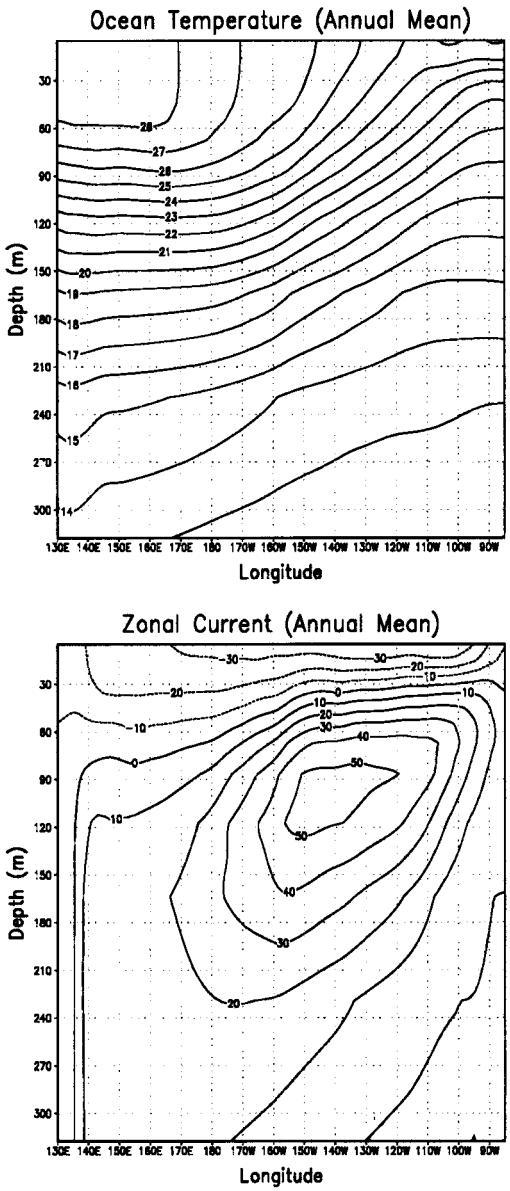

FIG. 5. Longitude–depth cross section of the simulated annual-mean ocean temperature (°C) and zonal ocean currents (cm s^{-1}) at the equator for case C.

depends strongly on the upper-ocean mean vertical temperature gradient, $\partial\overline{T}/\partial z$ [the second term at the right-hand side of Eq. (4.1)], it is efficient only in the eastern equatorial Pacific where the thermocline is shallow. The antisymmetric SST mode proposed by Chang and Philander (1994) has a zero amplitude right on the equator. To cause SST changes at the equator, an antisymmetry–symmetry conversion is required. This is done by anomalous meridional temperature advection [the third term on the right hand side of Eq. (4.1)] (Li and Philander 1996). If the annual-mean state were perfectly symmetrical (that is, $\overline{v} = \partial\overline{T}/\partial y = 0$), there would be no the antisymmetry–symmetry conversion.

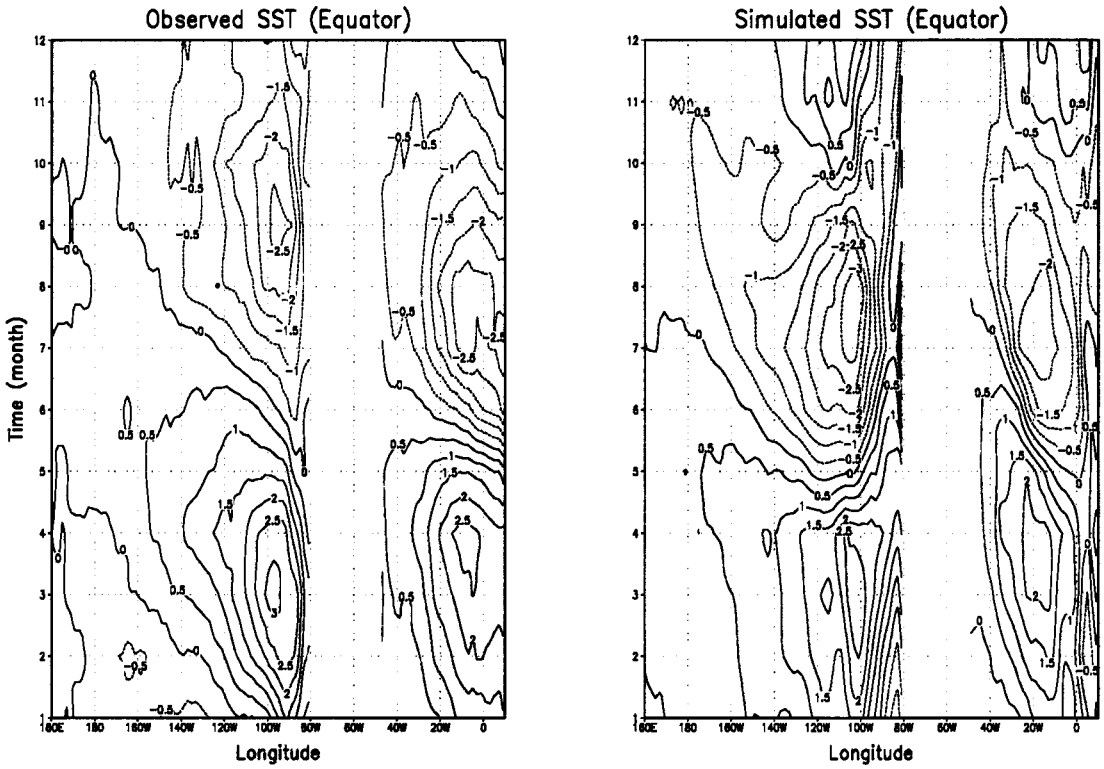

FIG. 6. Longitude–time section of the observed and simulated (case C) seasonal SST variations at the equator.

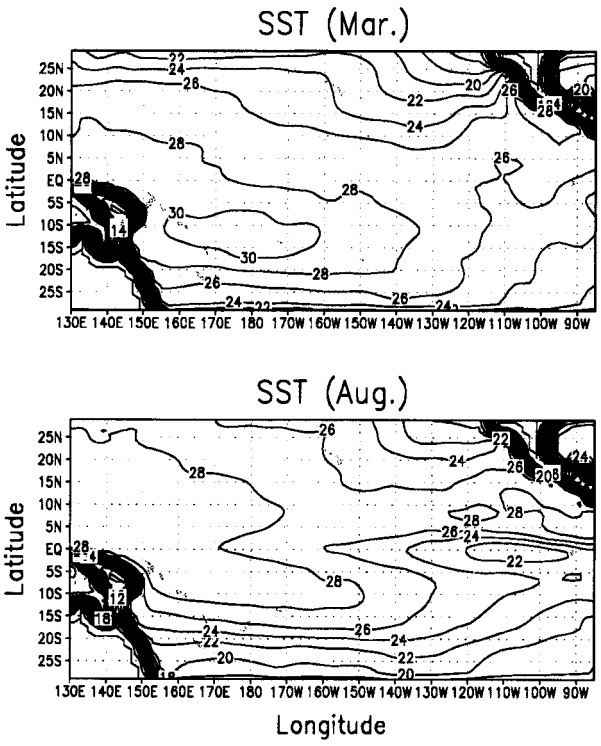

FIG. 7. Horizontal distribution of the simulated SST (°C) in Mar and Aug for case C.

Over the eastern tropical Pacific the clouds that have the largest effect are the low-level stratus off the coast of Peru and California. These clouds are particularly important because they involve a positive feedback: the more clouds there are, the colder the SST, the larger the atmospheric inversion, and the more clouds. This positive feedback can be readily seen from Eq. (4.1) (the last term on the right-hand side) since $C'_{\mathrm{STR}} \propto -T'$.

Equation (4.1) is a simple representation of the three types of air–sea feedback mechanisms: 1) the evaporation–wind feedback, 2) the meridional wind–SST feedback, and 3) the low-level stratus cloud–SST feedback. With the understanding of these processes, it is not difficult to explain why the simulated annual cycle in case A is unrealistic (Fig. 1).

The unrealistic annual cycle in case A is attributed to the unrealistic simulation of the annual-mean state. Figure 2 illustrates the horizontal maps of the simulated annual-mean SST and SST variations in the two extreme months of the seasonal cycle, March and August, for all three cases. A rather symmetric annual mean SST is found in the eastern equatorial Pacific (east of 120°W) in case A. Corresponding to this SST distribution, the northward cross-equatorial wind is much weaker because meridional SST gradients are weaker (Lindzen and Nigam 1987). This leads to less effective evaporation–wind feedback and the antisymmetry–symmetry conversion. The easterly trades are weaker too, because

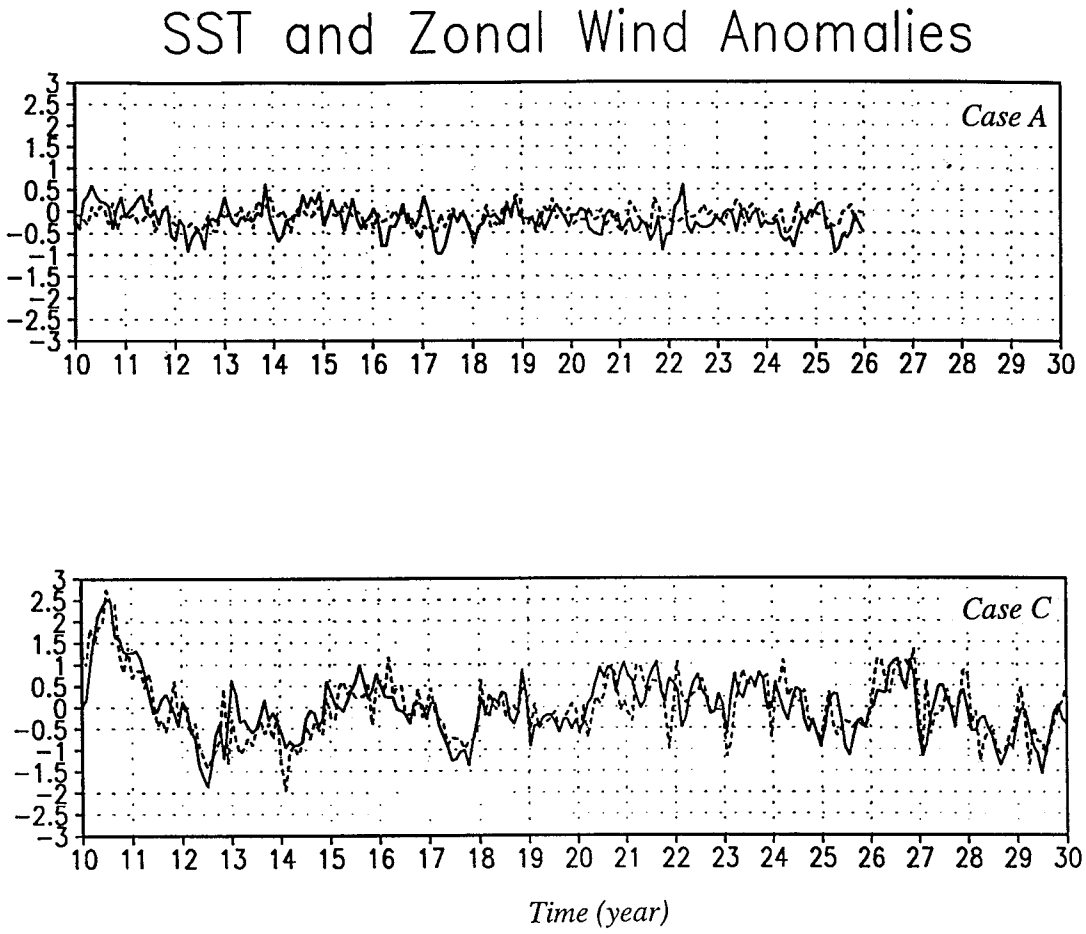

FIG. 8. Time series of the interannual SST (°C, 180°–100°W averaged) (the solid line) and zonal wind (m s^{-1}, 120°E–180° averaged) (the dashed line) anomalies at the equator for (top) case A and (bottom) case C.

of vanishing zonal SST gradients there. As a result, the ocean thermocline, represented by 20°C isothermal, has a large error toward the end of the eastern ocean boundary (Fig. 3). Since the dynamic air–sea coupling strongly depends on the upper-ocean thermal structure, the meridional wind–SST feedback is less effective. Also, the relatively high SST in the eastern equatorial Pacific prevents the formation of the low-level stratus clouds. All these factors attribute to the unsuccessful simulation of the annual cycle in this case.

In case B (the dotted line of Fig. 1), a realistic annual-mean SST distribution results in an improved simulation in both zonal and meridional wind fields and thus an improved ocean thermal structure (which, in turn, determines the strength of the coupled feedbacks). As a result, the evaporation–wind feedback and the meridional wind–SST feedback are more effective. The realistic low SST in the eastern equatorial Pacific also permits the formation of the low-level stratus clouds. The phase of this annual cycle is improved compared to case A, but the amplitude is still too weak (1.5°C) compared to the observed one (2.5°C) (see Fig. 1).

To obtain a realistic amplitude of the annual cycle of SST, an annual-mean wind adjustment appears to be needed. This is because even given a perfect SST distribution, the atmospheric model still generates errors in the surface wind fields. The most serious problem lies in the zonal wind component at the equator (Fig. 4). One can readily see from Fig. 4 that along the equatorial Pacific the model generally underestimates easterly trades to the east of 120°W, and overestimates them to the west of 120°W. Such an error has a significant impact on the upper-ocean thermocline structure. That is why the thermocline in case B, although improved compared to case A, still has errors in the eastern Pacific. A realistic description of the annual mean wind helps improve the ocean thermocline structure and surface latent and sensible heat fluxes, which leads to further improvement in the annual cycle simulation. The solid

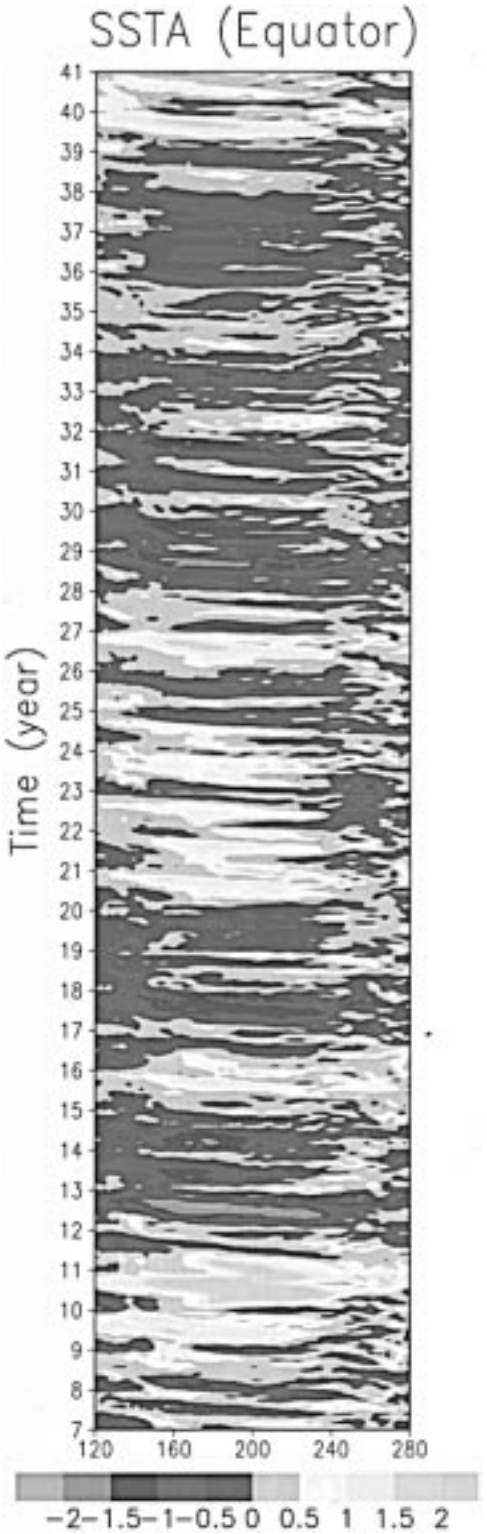

FIG. 9. Longitude–time section of the interannual SST anomalies (°C) at the equator for case C.

the depth of 120 m (Fig. 5). The amplitude of the undercurrents is 50–60 cm s^{-1}. A similar pattern is simulated in the equatorial Atlantic. The thermocline in the Indian Ocean, however, is uniformly deep along the equator. Correspondingly, there are no ocean undercurrents there.

One important feature of the annual cycle at the equator is the westward propagation in both SST and surface zonal wind fields (Horel 1982). This feature is well captured by our coupled model. Figure 6 shows both the observed and coupled model simulated SSTs at the equator. In general, the amplitude and phase of the annual SST variation in both the Pacific and Atlantic are well simulated, although in the eastern Pacific the cold phase of the SST is off by approximately 1 month.

For the seasonal cycle of the equatorial cold tongue, March and August are two extreme months. Figure 7 exhibits the horizontal distribution of the simulated SST fields in March and August for case C. There is indeed a strong contrast between the March and August SST fields. While the maximum SST in the eastern Pacific always stays north of the equator, it crosses the equator twice a year in the western Pacific, following the sun's movement. Correspondingly, the surface winds in the eastern equatorial Pacific are always toward the north, which converge onto the ITCZ, whereas in the western Pacific and Indian Ocean they change direction once a year, always blowing from the winter to the summer hemisphere (figure omitted).

5. The interannual variation simulation

It is well known from stability analysis (e.g., Hirst 1986; Neelin 1991; Wang and Feng 1996; Li 1997b) that the intensity and frequency of interannual coupled air–sea modes strongly depend on basic-state atmospheric and oceanic conditions such as the upper-ocean mean vertical temperature gradients (or stratification), mean upwelling, and the mean depth of the ocean thermocline. The coupled model experiments by Zebiak and Cane (1987) and Latif et al. (1993) demonstrate that interannual oscillations are very sensitive to the zonal mean thermocline depth and that even a modest increase in the background wind stress may entirely suppress the interannual variability in their models.

Our long-term simulations indicate that the interannual oscillations in the model are sensitive to the model basic states. Figure 8 shows that the amplitude of the interannual SST (averaged between 180°–120°W) and zonal wind (averaged between 120°E–180°) anomalies in case A are much weaker than that in case C. (The reason to choose the different averaging regions for the SST and wind is based on the observational fact that maximum interannual wind anomalies are located in the western and central equatorial Pacific whereas maximum SST anomalies are in the eastern equatorial Pacific.) The dependence of the model interannual oscillations on the basic states does not imply that ocean

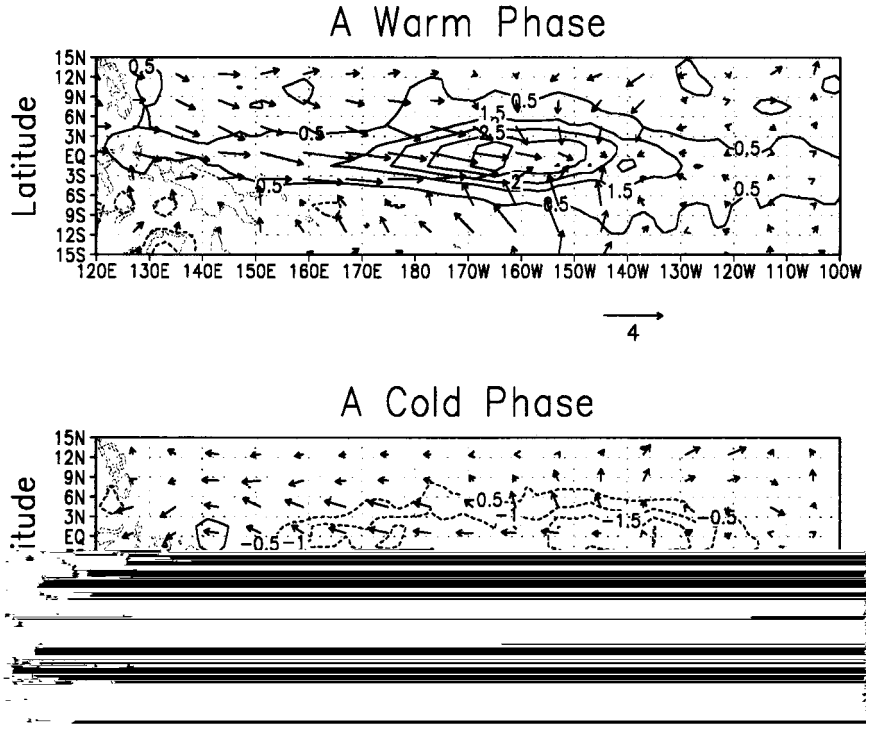

FIG. 10. Horizontal structure of the interannual SST (°C) and surface wind (m s^{-1}) anomalies during a typical warm (at month 8 of year 10) and cold (at month 8 of year 12) event for case C.

dynamics that involve the equatorial waveguide and thermocline changes are not important. Rather it reflects the role of basic state conditions on the strength of air–sea coupling.

Figure 9 illustrates the time–longitude section of interannual SST anomalies at the equator for case C. The maximum interannual SST anomalies exceed 2°C. While the large interannual variability is found in the equatorial Pacific, much weaker interannual variability is simulated in the equatorial Atlantic (figure omitted). This agrees with observations.

The interannual variations in the model result from the strong coupling between the atmosphere and ocean. Figure 10 exhibits the horizontal structure of the anomalous SST and surface wind fields during a typical warm (month 8 of year 10) and cold (month 8 of year 12) event. In response to anomalous heat source induced by the anomalous warm SST across the equatorial Pacific, a weakened Walker circulation is established. Maximum surface westerly anomalies appear to the west of the warm SST anomaly. The winds converge onto the warm SST anomaly region. During a cold event a negative anomalous heat source causes the divergence of surface wind anomalies. Easterly wind anomalies appear to the west of a cold SST anomaly. Such horizontal patterns agree with the observed El Niño and La Niña conditions.

So far three ENSO phase transition mechanisms have been proposed. The first one is the delayed oscillator mode (Schopf and Suarez 1988; Battisti and Hirst 1989) that emphasizes the propagation of equatorial ocean (Rossby and Kelvin) waves and the reflection of those waves in the western boundary. The second one is the slow SST mode (Neelin 1991) that emphasizes the zonal propagation of SST along the equator. The third one is the stationary SST mode (Li 1997b), termed the ''ocean recharge–discharge mode'' by Jin (1997), that emphasizes the disequilibrium between the zonal mean thermocline depth and surface wind anomalies.

Diagnoses of the coupled model results indicate that the interannual oscillations in the model capture essentially all three modes. Figure 11 shows the evidence of the delayed oscillator mode. It illustrates the time–longitude profile of the upper-ocean-heat content (defined as the vertical integration of ocean temperatures from surface to 320 m) anomalies at the equator and along 8°N and 8°S. Along the equator there is clearly eastward propagation in the heat content field. The speed of the eastward propagation is approximately 0.6 m s^{-1}. Off the equator it propagates westward, at a speed of 0.2 m s^{-1}. The propagation speeds are much smaller compared to those of free equatorial oceanic Kelvin and Rossby waves, and thus represent the slow coupled modes discussed by Hirst (1986) and Schopf and Suarez (1988). The reflection of the waves in the western boundary may be deduced from Fig. 11 in which one can see the connection between the slow westward-propagating Rossby-type waves off the equator and the slow eastward Kelvin-type waves at the equator at years 12, 16,

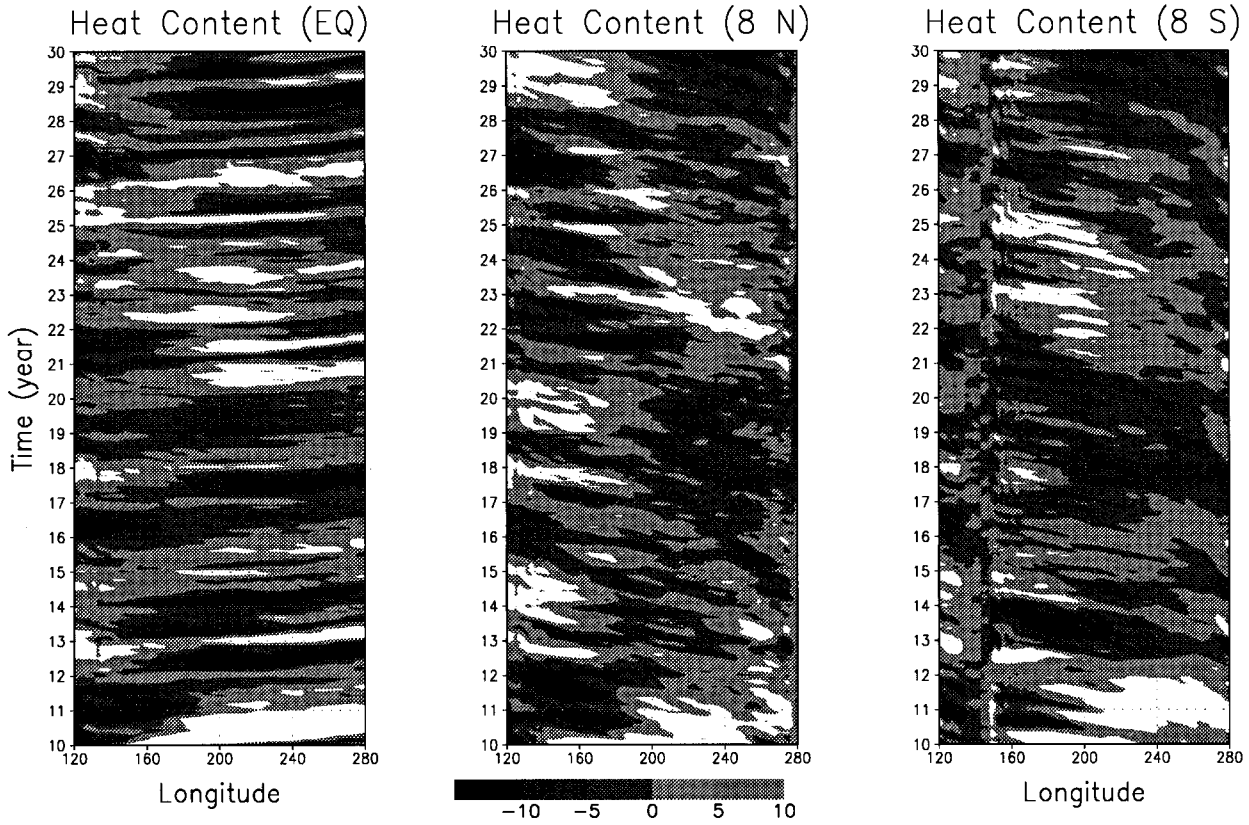

FIG. 11. Longitude–time section of the upper-ocean heat content anomalies (units: 10 °C m) at the equator and along 8°N and 8°5 for case C.

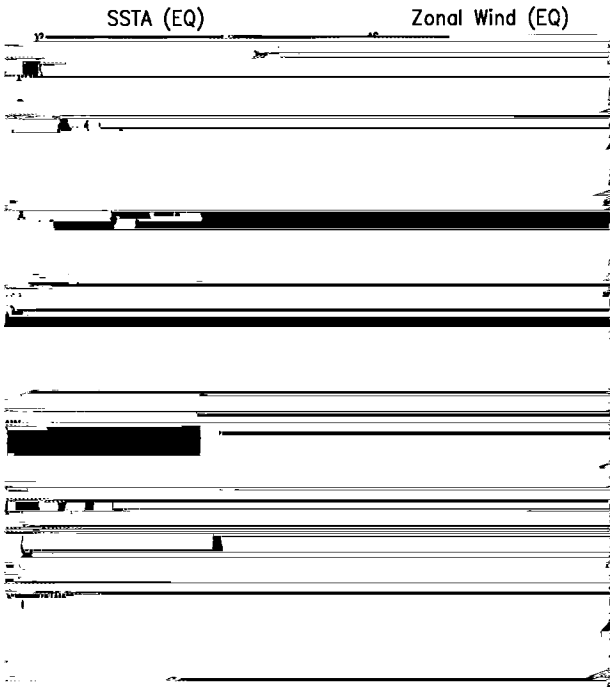

FIG. 12. Longitude–time section of the SST (°C) and zonal wind (m s^{-1}) anomalies along the equator (at year 12) for case C.

19, 21, 22, and 27. In addition to the delayed oscillator mode, there is the evidence of the zonally propagating slow SST mode. Figure 12 shows SST and zonal wind anomalies along the equator for a typical cold event at year 12. Both the SST and surface zonal wind anomalies propagate westward. The phase speed of the propagation is approximately 15° long $month^{-1}$. The stationary SST mode is characterized by the zonal mean thermocline depth anomaly leading the SST (or wind) anomaly at the equator (see Fig. 3 of Li 1997b). Figure 13 shows that the zonal mean thermocline depth anomaly in the model indeed leads the SST anomaly in some periods (e.g., at years 10–11 and years 26–27). These results suggest that the coupled model captures essentially all three types of ENSO modes.

6. Summary and discussion

A critical feature for all coupled ocean–atmosphere GCMs is the ability to simulate both seasonal and interannual variations. We investigate the role of the annual-mean climate on seasonal and interannual variability by means of a coupled ocean–atmosphere GCM. The atmospheric component of this coupled GCM is the Naval Operational Global Atmospheric Prediction System and the oceanic component is the Geophysical Fluid Dynamics Laboratory Modular Ocean Model. Three sets

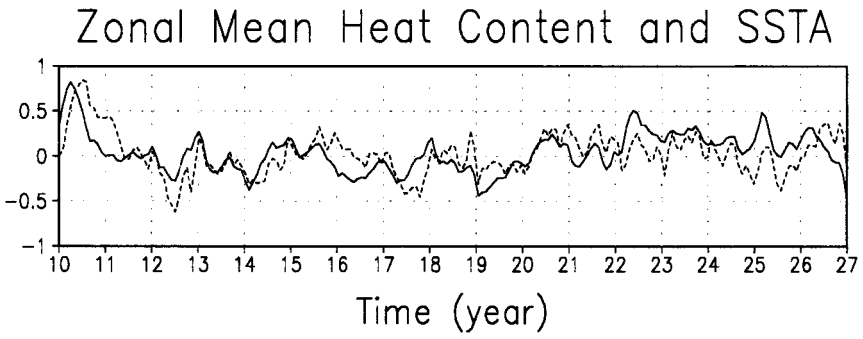

FIG. 13. Time series of the zonal-mean heat content anomaly (units: 150 °C m, the solid line) and the SST anomaly (units: 3°C, averaged between 180° and 100°W); the dashed line) at the equator for case C.

of experiments have been carried out. In case A, no annual-mean flux adjustment is applied so that the coupled model generates its own time-mean state. In case B, a constant annual-mean flux adjustment for SST is applied. In case C, both the annual-mean SST and surface wind fields are adjusted. Our long-term (40 yr) simulations of the coupled GCM demonstrate that in the presence of the annual-mean SST and surface wind adjustment, the coupled model is able to simulate realistic seasonal and interannual variations in the tropical Pacific. Particularly, it simulates the westward propagation of the seasonal SST variations along the equator. The structure of the simulated interannual oscillations resembles in many aspects that of the El Niño and Southern Oscillation. It is concluded that a prerequisite for a coupled GCM to simulate/predict realistic seasonal and interannual variations is to simulate a realistic annual-mean state.

The conclusion derived from the coupled experiments is consistent with previous theoretical and observational studies. It has been long noticed from an observational point of view that the phase of the El Niño and Southern Oscillation is closely related to the seasonal cycle (e.g., Rasmusson and Carpenter 1982). The sensitivity experiments by Zebiak and Cane (1987) indicated that irregular interannual oscillations can emerge when a seasonally varying, rather than an annual-mean, basic state is specified. Li and Philander (1996) demonstrated that the principal cause of an annual cycle at the equator is the asymmetric annual-mean climate.

The drift of the time-mean equilibrium state away from the observed climate is clearly a sign that something is amiss in the atmospheric and oceanic models. The diagnosis of the annual-mean heat flux adjustment fields (Fig. 14) points to certain key physical processes in the models. For instance, in both fixed SST and coupled experiments, deep convective clouds over the western tropical Pacific are generally overpredicted. Those clouds reflect too much solar radiation to the space and cause cooler SSTs there. The low-level stratus clouds along the coast of the South America are underestimated, leading to excess of solar irradiance and consequently too warm SSTs. The ocean upwelling is in general too weak in the far eastern equatorial Pacific and along the coast of the South America but too strong along the central equatorial Pacific. A large cold bias in SST is found off the coast of the Central America. The reason for such a bias is currently under investigation.

The fact that the coupled equilibrium state severely deviates from real climate does not necessarily imply that the model dynamics are too unrealistic to be used for climate variability and sensitivity experiments. The success in simulating both seasonal and interannual variations in the current coupled GCM poses an interesting question: can we apply the annual-mean flux adjustment strategy to conduct long-term (seasonal and interannual) climate forecasts? There are, in general, two approaches to solve the annual-mean errors in a coupled model. One is to apply an annual-mean adjustment approach, as proposed by this study. Another is to improve the model physics such as the better representation of cumulus clouds over the western equatorial Pacific and shallow low stratus clouds off the coasts of Peru. The former is expedient, whereas the later is slow but essential. We believe that both strategies are important. By applying the annual-mean adjustment strategy, we can avoid the time-mean problems and go forward to consider other important issues such as nonlinear interactions between seasonal and interannual timescales and the predictability of coupled GCMs.

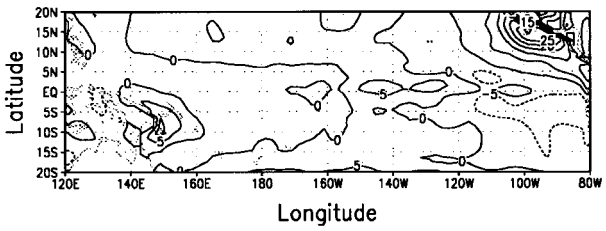

FIG. 14. Horizontal map of the annual-mean heat flux adjustment term for SST (units: (10^{-7}°C s^{-1}) in case C.

Acknowledgments. The authors would like to thank Dr. Inez Fung and two anonymous reviewers for their constructive comments that helped improve the manuscript. This study is supported by the Office of Naval Research and Naval Research Laboratory under program element 0601153N.

REFERENCES

Battisti, D. S., and A. C. Hirst, 1989: Interannual variability in the tropical atmosphere–ocean system: Influence of the basic state and ocean geometry. *J. Atmos. Sci.,* **46,** 1687–1712.

Bjerknes, J., 1966: A possible response of the atmospheric Hadley circulation to equatorial anomalies of ocean temperature. *Tellus,* **18,** 820–829.

——, 1969: Atmospheric teleconnections from the equatorial Pacific. *Mon. Wea. Rev.,* **97,** 163–172.

Bryan, K., 1969: A numerical method for the study of the circulation of the world ocean. *J. Comput. Phys.,* **4,** 347–376.

Cane, M., and S. E. Zebiak, 1985: A theory for El Niño and the Southern Oscillation. *Science,* **228,** 1084–1087.

Chang, P., and S. G. H. Philander, 1994: A coupled ocean–atmosphere instability of relevance to seasonal cycle. *J. Atmos. Sci.,* **51,** 3627–3648.

——, B. Wang, T. Li, and L. Ji, 1994: Interactions between the seasonal cycle and the Southern Oscillation—Frequency entrainment and chaos in a coupled ocean–atmosphere model. *Geophys. Res. Lett.,* **21,** 2817–2820.

——, L. Ji, B. Wang, and T. Li, 1995: On the interactions between the seasonal cycle and El Niño–Southern Oscillation in an intermediate coupled ocean–atmosphere model. *J. Atmos. Sci.,* **52,** 2353–2372.

Chao, Y., and S. G. H. Philander, 1993: On the structure of the Southern Oscillation. *J. Climate.,* **6,** 450–469.

Dukowicz, J. K., and R. D. Smith, 1994: Implicit free-surface method for the Bryan-Cox-Semtner ocean model. *J. Geophys. Res.,* **99,** 7991–8014.

Frey, H., M. Latif, and T. Stockdale, 1997: The coupled GCM ECHO-2. Part I: The tropical Pacific. *Mon. Wea. Rev.,* **125,** 703–720.

Gu, D., and S. G. H. Philander, 1995: Secular changes of annual and interannual variability in the tropics during the past century. *J. Climate,* **8,** 864–876.

Harshvardhan, R. Davies, D. Randall, and T. Corsetti, 1987: A fast radiation parameterization for atmospheric circulation models. *J. Geophys. Res.,* **92,** 1009–1016.

Hirst, A. C., 1986: Unstable and damped equatorial modes in simple coupled ocean–atmosphere models. *J. Atmos. Sci.,* **43,** 606–630.

Hogan, T. F., and T. E. Rosmond, 1991: The description of the Navy Operational Global Atmospheric Prediction System's spectral forecast model. *Mon. Wea. Rev.,* **119,** 1786–1815.

Horel, J. D., 1982: On the annual cycle of the tropical Pacific atmosphere and ocean. *Mon. Wea. Rev.,* **110,** 1863–1878.

Ineson, S., and M. K. Davey, 1997: Interannual climate simulation and predictability in a coupled TOGA GCM. *Mon. Wea. Rev.,* **125,** 721–741.

Ji, M., and A. Leetmaa, 1994: An improved coupled ocean–atmosphere model for ENSO predictions. *Proc. 19th Climate Diagnostic Workshop,* College Park, MD, NOAA, 88–91.

Jin, F.-F., 1997: An equatorial ocean recharge paradigm for ENSO. Part I: Conceptual model. *J. Atmos. Sci.,* **54,** 811–829.

——, J. D. Neelin, and M. Ghil, 1994: El Niño on the devil's staircase: Annual subharmonic steps to chaos. *Science,* **264,** 70–72.

Latif, M., J. Biercamp, H. von Storch, and F. W. Zwiers, 1988: A ten-year climate simulation with a coupled ocean–atmosphere general circulation model. Max-Planck Institut für Meteorologie Rep. 21. [Available from Max-Planck Institut für Meteorologie, Bundesstraße 55, D-2000 Hamburg 13, Germany.]

——, A. Sterl, E. Maier-Reimer, and M. M. Junge, 1993: Climate variability in a coupled GCM. Part I: The tropical Pacific. *J. Climate,* **6,** 5–21.

Levitus, S., 1982: *Climatological Atlas of the World Ocean.* NOAA Professional Paper 13, 173 pp. and 17 microfiche.

Li, T., 1997a: Air–sea interactions of relevance to the ITCZ: Analysis of coupled instabilities and experiments in a hybrid coupled GCM. *J. Atmos. Sci.,* **54,** 134–147.

——, 1997b: On the phase transition of the El Niño–Southern Oscillation: A stationary SST mode. *J. Atmos. Sci.,* **54,** 2872–2887.

——, and S. G. H. Philander, 1996: On the annual cycle of the eastern equatorial Pacific. *J. Climate,* **9,** 2986–2998.

——, and ——, 1997: On the seasonal cycle of the equatorial Atlantic. *J. Climate,* **10,** 813–817.

Lindzen, R. S., and S. Nigam, 1987: On the role of sea surface temperature gradients in forcing low-level winds and convergence in the Tropics. *J. Atmos. Sci.,* **44,** 2240–2458.

Louis, J. F., M. Tiedtke, and J. F. Geleyn, 1982: A short history of the operational PBL parameterization at ECMWF. *Proc. Workshop on Planetary Boundary Layer Parameterization,* Reading, United Kingdom, ECMWF, 59–79.

Manabe, S., and R. J. Stouffer, 1996: Low-frequency variability of surface air temperature in a 1000-year integration of a coupled atmosphere–ocean–land surface model. *J. Climate,* **9,** 376–393.

McCreary, J. P., 1983: A model of tropical ocean–atmosphere interaction. *Mon. Wea. Rev.,* **111,** 370–387.

Mechoso, M. R., and Coauthors, 1995: The seasonal cycle over the tropical Pacific in coupled ocean–atmosphere general circulation models. *Mon. Wea. Rev.,* **123,** 2825–2838.

Mitchell, T. P., and J. M. Wallace, 1992: On the annual cycle in equatorial convection and sea surface temperature. *J. Climate,* **5,** 1140–1152.

Miyakoda, K., J. Sirutis, A. Rosati, and J. Derber, 1990: Experimental seasonal forecasts with an air–sea model—Preliminary results. *Air–Sea Interaction in Tropical Western Pacific,* J.-P. Chao and J. A. Young, Eds., China Press, 417–432.

Moorthi, S., and M. J. Suarez, 1992: Relaxed Arakawa–Schubert: A parameterization of moist convection for general circulation models. *Mon. Wea. Rev.,* **120,** 978–1002.

Neelin, J. D., 1991: The slow sea surface temperature mode and the fast-wave limit: Analytic theory for tropical interannual oscillation and experiments in a hybrid coupled model. *J. Atmos. Sci.,* **48,** 584–606.

——, and Coauthors, 1992: Tropical air–sea interactions in general circulation models. *Climate Dyn.,* **7,** 73–104.

Pacanowski, R. C., 1995: MOM 2 documentation, user's guide and reference manual. GFDL Ocean Tech. Rep. 3, GFDL, Princeton, NJ, 232 pp.

——, and S. G. H. Philander, 1981: Parameterization of vertical mixing in numerical models of the tropical ocean. *J. Phys. Oceanogr.,* **11,** 1442–1451.

Palmer, T. N., G. J. Shutts, and R. Swinbank, 1986: Alleviation of a systematic westerly bias in general and numerical weather prediction models through an orographic gravity wave drag parameterization. *Quart. J. Roy. Meteor. Soc.,* **112,** 1001–1039.

Philander, S. G. H., 1990: *El Niño, La Niña, and the Southern Oscillation.* Academic Press, 293 pp.

——, and R. C. Pacanowski, 1981: The response of equatorial oceans to periodic forcing. *J. Geophys. Res.,* **86,** 1903–1916.

——, and A. D. Seigel, 1985: Simulation of El Niño of 1982–1983. *Coupled Ocean–Atmosphere Models,* J. G. J. Nihoul, Ed., Elsevier Oceanography Series, Vol. 40, Elsevier, 517–541.

——, T. Yamagata, and R. C. Pacanowski, 1984: Unstable air–sea interaction in the Tropics. *J. Atmos. Sci.,* **41,** 604–613.

——, R. C. Pacanowski, N. C. Lau, and M. J. Nath, 1992: Simulation of ENSO with a global atmospheric GCM coupled to a high-resolution, tropical Pacific Ocean GCM. *J. Climate,* **5,** 308–329.

——, D. Gu, D. Halpern, G. Lambert, G. Lau, T. Li, and R. C. Pacanowski, 1996: Why the ITCZ is mostly north of the equator. *J. Climate,* **9,** 2958–2972.

Rasmusson, E. M., and T. H. Carpenter, 1982: Variations in tropical

sea surface temperature and surface wind fields associated with the Southern Oscillation–El Niño. *Mon. Wea. Rev.,* **110,** 354–384.

Robertson, A. W., C.-C. Ma, C. R. Mechoso, and M. Ghil, 1995a: Simulation of the tropical Pacific climate with a coupled ocean–atmosphere general circulation model. Part I: The seasonal cycle. *J. Climate,* **8,** 1178–1198.

——, ——, M. Ghil, and C. R. Mechoso, 1995b: Simulation of the tropical Pacific climate with a coupled ocean–atmosphere general circulation model. Part II: Interannual variability. *J. Climate,* **8,** 1199–1216.

Sadler, J. C., M. A. Lander, A. M. Hori, and L. K. Oda, 1987: Tropical marine climatic atlas, Vol. 2, Pacific Ocean. UHMET Rep. 87-02, 27 pp. [Available from Department of Meteorology, University of Hawaii, Honolulu, Hawaii.]

Sausen, R., K. Barthel, and K. Hasselmann, 1988: Coupled ocean–atmosphere models with flux correction. *Climate Dyn.,* **2,** 145–163.

Schneider, E. K., and Coauthors, 1997: Annual cycle and ENSO in a coupled ocean–atmosphere general circulation model. *Mon. Wea. Rev.,* **125,** 680–702.

Schopf, P. S., and M. J. Suarez, 1988: Vacillations in a coupled ocean–atmosphere model. *J. Atmos. Sci.,* **45,** 549–566.

Slingo, J., 1987: The development and verification of a cloud prediction scheme for the ECMWF model. *Quart. J. Roy. Meteor. Soc.,* **113,** 899–927.

Tiedtke, M., 1984: The sensitivity of the time-scale flow to cumulus convection in the ECMWF model. *Proc. Workshop on Convection in Large Scale Numerical Models,* Reading, United Kingdom, ECMWF, 297–316.

Tziperman, E., L. Stone, M. Cane, and H. Jarosh, 1994: El Niño chaos: Overlapping of resonances between the seasonal cycle and the Pacific ocean-atmosphere oscillator. *Science,* **264,** 72–74.

Wang, B., 1994: On the annual cycle in the tropical eastern–central Pacific. *J. Climate,* **7,** 1926–1942.

——, and Z. Feng, 1996: Chaotic oscillations of tropical climate: A dynamic system theory for ENSO. *J. Atmos. Sci.,* **53,** 2786–2802.

Wyrtki, K., 1975: El Niño—The dynamic response of the equatorial Pacific Ocean to atmospheric forcing. *J. Phys. Oceanogr.,* **5,** 572–584.

Xie, S.-P., and S. G. H. Philander, 1994: A coupled ocean–atmosphere model of relevance to the ITCZ in the eastern Pacific. *Tellus,* **46A,** 340–350.

Zebiak, S. E., and M. A. Cane, 1987: A model ENSO. *Mon. Wea. Rev.,* **115,** 2262–2278.